AIMS Environmental Science

AIMS Environmental Science, 11(4): 576–592.
DOI: 10.3934/environsci.2024028
Received: 02 May 2024
Revised: 09 July 2024
Accepted: 17 July 2024
Published: 25 July 2024

https://www.aimspress.com/journal/environmental

Research article

Optimizing the synthesis conditions of aerogels based on cellulose fiber extracted from rambutan peel using response surface methodology

Nguyen Trinh Trong[1,2], Phu Huynh Le Tan[1], Dat Nguyen Ngoc[1], Ba Le Huy[2], Dat Tran Thanh[3] and Nam Thai Van[4,*]

[1] HUTECH Institute of Applied Sciences, HUTECH University, Ho Chi Minh City, Vietnam; tt.nguyen@hutech.edu.vn, phucleotoanhuynh@gmail.com, ngocdat200199@gmail.com

[2] Faculty of Biology and Environment, Ho Chi Minh City University of Industry and Trade (HUIT), 140 Le Trong Tan Street, Tay Thanh Ward, Tan Phu District, Ho Chi Minh City 70000, Vietnam; 6009220001@huit.edu.vn, lhuyba@gmail.com

[3] HCMC Industry and Trade College (HITC), Vietnam; dattranthanh9@gmail.com

[4] Institute of Postgraduate Studies, HUTECH University, Ho Chi Minh City, Vietnam; tv.nam@hutech.edu.vn

*** Correspondence:** Email: tv.nam@hutech.edu.vn; Tel: +84945007990.

Abstract. A cellulose-based aerogel has been synthesized from rambutan peel to mitigate environmental pollution caused by agricultural waste, rendering it an eco-friendly material with potential applications in oil spill remediation as well as enhancing the value of this fruit. The objective of this study was to extract cellulose from rambutan peel using chlorination and alkalization processes, followed by optimizing the synthesis conditions of cellulose-based aerogels from rambutan peel through experimental designs to improve oil removal efficiency. In this research, cellulose-based aerogel material was synthesized using the sol-gel method, utilizing waste from rambutan peel as the substrate and polyvinyl alcohol as the cross-linking agent, followed by freeze-drying. A central composite design with 30 different experimental setups was employed to investigate the influence of cellulose content (1.0–2.0%), cross-linking agent (polyvinyl alcohol) content (0.1–0.3%), ultrasonic

time (5–15 min), and ultrasonic power (100–300W) on the oil adsorption capacity (g/g) of cellulose-based aerogels from rambutan peel. The research findings demonstrated successful extraction of cellulose from rambutan peel through chlorination, followed by softening with 17.5% (w/v) sodium hydroxide. Response surface plots indicated that maximizing the cellulose component could lead to a maximum diesel oil adsorption capacity of up to 52.301 g/g. Cellulose-based aerogel exhibits ultra-lightweight properties (0.027±0.002 g/cm^3), high porosity (97.88±0.19), hydrophobicity (water contact angle of 152.7^o), and superior oil selective adsorption compared to several commercially available materials in the market, demonstrating promising potential for application in treating oil-contaminated water in real-world scenarios.

Keywords: agricultural waste; cellulose-based aerogel; green materials; oil spill remediation; rambutan peel

1. Introduction

Contaminated water with oil poses a significant global threat to water quality and underwater ecosystems, leading to severe health consequences [1]. Various techniques are employed to eliminate oil from aquatic environments, ranging from in-situ burning and chemical methods (solidification and dispersion) to biological approaches and physical techniques such as skimming and the use of absorbents [2]. Among these, natural organic adsorbents offer distinct advantages over other materials, particularly in terms of environmental compatibility in marine settings and their lightweight nature, which facilitates easy retrieval and reuse [3].

In recent years, materials research has increasingly emphasized the development of eco-friendly and multifunctional materials. Aerogels have emerged as a highly versatile and valuable engineering material due to their exceptional properties, such as extremely low density (0.001–0.5 g/cm^3), high porosity (95–99%), and expansive specific internal surface area (10–2000 m^2/g) [4]. Of particular interest are recycled cellulose aerogels, which have garnered significant attention for their broad applications in absorption, oil/water separation, thermal and acoustic insulation, and numerous other technical fields [5–8].

The rambutan (*Nephelium lappaceum* L.) is native to Indonesia, Malaysia, and southern Thailand. It is cultivated extensively in Malaysia, Thailand, the Philippines, northern Australia, Sri Lanka, India, Madagascar, Costa Rica, the Congo, and several South American countries. Thailand, Malaysia, and Indonesia are the world's largest producers of rambutan, accounting for over 90% of the global supply [9]. In Vietnam, rambutan is also a popular fruit and is ranked among the top ten main fruit crops [10]. According to the Ministry of Agriculture and Rural Development's review and data from the General Statistics Office, Vietnam's rambutan production in 2023 reached 325,000 tons, marking an increase of 3.4% [11]. Rambutan peel (RP) is considered as an agricultural byproduct containing a significant cellulose content, reaching 24.28% [12], making it a cost-effective and economically viable

material for oil adsorption in water.

The response surface methodology (RSM) is a mathematical and statistical approach utilized in experimental design [13]. This method assumes that the response surface can describe the relationship between experimental factors and measured responses, aiming to determine optimal factor settings to achieve an optimal response [14], while also indicating how the response varies in a particular direction by adjusting design variables [15]. RSM is widely applied in optimizing conditions for multivariate systems based on central composite design (CCD) [16]. Meng and et al. have demonstrated its effectiveness in optimizing the manufacturing process of carbon aerogels from nanocellulose fibers [17].

In this research, rambutan peel will be selected as the primary material for the production of affordable and eco-friendly oil-absorbent materials. The aerogels will be synthesized using the freeze-drying method to save time compared to conventional sol-gel methods. Furthermore, the design of experiment (DOE) method will be utilized to investigate the factors influencing the aerogel synthesis process, aiming to enhance efficiency compared to conventional single-factor optimization methods, which are known for being time-consuming and expensive while providing vague and misleading information.

2. Materials and methods

2.1. Materials

The rambutan peel was obtained from a main market in Ho Chi Minh City, Vietnam, while diesel oil 0.05S, with a specific gravity at 15^{o}C ranging from 820 to 860 kg/m^3, was acquired from Petrolimex Aviation, also based in HCMC, Vietnam. Sodium chlorite $NaClO_2$ 80% and methyltrimethoxysilane (MTMS) were imported from China. Acetic acid (glacial) 100% Merck, boasting a density of 1.04 g/cm^3 at 25^{o}C, was utilized. Sodium hydroxide (>96% NaOH), packaged in 500g bottles by Xi-long, was employed. PVA (polyvinyl alcohol), fully hydrolyzed for synthesis, 100g by Merck, presented a density of 1.3 g/cm^3 at 20^{o}C. Deionized water was utilized throughout the experiments.

2.2. Extraction of cellulose from rambutan peel

Cellulose fibers (RPF-C) were derived from raw rambutan peel fibers (RPF-R) using a two-step method described by Penjumras et al., 2014. This process involved initially creating holocellulose through either chlorination or bleaching. In the first step, 20 g of RPF-R were immersed in 640 mL of distilled water in a 1000 mL glass beaker. Over a period of 5 hours, 4 mL of CH_3COOH and 8 g of $NaClO_2$ were incrementally added to the beaker to eliminate lignin from the fibers. Following this, the sample was left to soak overnight in a thermostatic bath set at 60^{o}C. Subsequent rinsing with tap water until a yellow hue emerged (in contrast to the white color of holocellulose) and complete removal of the chlorine dioxide odor indicated the completion of this step.

The second phase involved converting holocellulose into cellulose via alkali treatment at ambient temperature. The holocellulose obtained from the previous step was mixed with 80 mL of 17.5% NaOH solution and stirred thoroughly. Every 5 minutes, 40 mL of another 17.5% NaOH solution was added to the mixture in three intervals. After 30 minutes of standing, totaling 45 minutes of NaOH treatment, 240 mL of distilled water was added and left to stand for 1 hour before filtration and rinsing. The resulting alkali-treated cellulose was neutralized by the addition of 120 mL of 10% CH_3COOH over 5 minutes. Finally, the cellulose was filtered, rinsed with distilled water until neutral, and dried overnight at 80^{o}C. The weight of the recovered cellulose was recorded, and its percentage recovery was calculated using formula (1). The cellulose fibers were stored in a sealed container at room temperature and prepared for subsequent analysis [18].

$$\boldsymbol{Cellulose}\ (\%) = \frac{\boldsymbol{W_2}}{\boldsymbol{W_1}} \times \mathbf{100} \tag{1}$$

In which, W_1 = Weight of RPF-R (g) and W_2 = Weight of RPF-C (g).

2.3. Preparation of adsorbent aerogel

RPF-C obtained from the previous processing step is mixed with deionized water for at least 1 hour to form a homogeneous suspension [19]. Subsequently, a 5% PVA solution is dispersed into the RPF-C mixture in order to achieve the desired concentration. The mixture is then sonicated using an UP400St Hielscher ultrasonic homogenizer from Germany. The ultrasonic treatment is conducted in an ice-water bath. The resultant mixture is subsequently refrigerated and subjected to freezing at -4^{o}C for 24 hours. RP aerogels are produced by freeze-drying under a pressure of 0.5 mbar for 48 hours utilizing a vacuum freeze dryer [20]. Finally, the samples are annealed at 120^{o}C for 3 hours to promote cross-linking and form a three-dimensional network [17].

2.4. Preparation of hydrophobic adsorbent aerogel

The RP aerogel samples are placed in a large glass container containing a glass vial pre-filled with 5 mL of MTMS (with the lid open). The glass container containing the RP aerogels is tightly sealed and placed in an oven at 80^{o}C for 3 hours. Upon completion of the reaction, the glass container is placed in a desiccator, the lid is opened, and it is vacuumed for 30 minutes to remove excess MTMS [21].

2.5. Experimental design for optimization

Experiments for optimization are commonly designed using RSM, with the CCD being the most prevalent. CCD is extensively applied in the development of second-order response surface models. It stands as one of the most crucial experimental design methods employed in optimization research processes [22].

Herein, the CCD consists of 2^n factorial trials, supplemented by $2n$ axial runs and n_c center runs.

The central points are utilized to assess experimental variability and data replicability, whereas the axial points guarantee rotational symmetry to uphold a consistent variance of model forecasts equidistant from the design core [23]. Consequently, in accordance with Owolabi RU et al' study [24], the requisite count of experimental trials can be computed employing Eq 2.

$$N = 2^n + 2n + n_c = 2^4 + 2 \times 4 + 6 = 30 \quad (2)$$

where N represents the total count of experimental trials, n denotes the number of factors, and n_c signifies the number of central points.

In this investigation, the factors examined were as follows: cellulose content (A), PVA content (B), ultrasonic time (C), and ultrasonic power (D). The response was the oil adsorption capacity (Y). The analysis of the response surface methodology (RSM) model employed the central composite design (CCD) generated by Design-Expert 13 software. The ranges of the factors are detailed in Table 1.

Table 1. Ranges of factors for the experimental design.

Factors	Symbol	-α	Low	Center	High	+α	Unit
Level		-2	-1	0	1	2	
Cellulose content	A	0.5	1	1.5	2	2.5	%wt
PVA content	B	0	0.1	0.2	0.3	0.4	%wt
Ultrasonic time	C	0	5	10	15	20	min
Ultrasonic power	D	0	100	200	300	400	W
Response							
Oil adsorption capacity	Y						g/g

RSM is grounded in experimental techniques utilized to explore the relationship between experimental factors and measured responses. RSM effectively elucidates the connections between independent variables and dependent variables [25]. Mathematically, this relationship is expressed through the following Eq 3 [26]:

$$\boldsymbol{y = \beta_0 + \sum_{i=1}^{k} \beta_i x_i + \sum_{i=1}^{k} \beta_{ii} x_i^2 + \sum_{1 \le i \le j}^{k} \beta_{ij} x_i x_j + \varepsilon} \quad (3)$$

where k represents the number of input variables, x_i denotes the input variables (independent variables), y is the output variable (response or dependent variable), β_0 is the constant term, β_i are the coefficients of the linear terms, β_{ii} are the coefficients of the quadratic terms, β_{ij} are the coefficients of the interaction terms between input variables, and ε is the error term associated with the experiment.

2.6. Characterization of adsorbent

SEM analyses were conducted using the JSM-IT500 InTouchScope™ Scanning Electron Microscope, while FT-IR measurements were carried out employing the Agilent Cary 630 FTIR

spectrometer.

The apparent density of the RP aerogels is assessed by measuring and calculating the ratio between the mass and volume of the RP aerogels using Eq 4 [27].

$$\boldsymbol{\rho_a = \frac{m}{\frac{2\pi DH}{4}}} \tag{4}$$

in which ρ_a is the density of the aerogel (g/cm^3), m is the mass of the aerogel (gram), D is the diameter of the cross-section of the aerogel (cm), and H is the height of the aerogel (cm).

The porosity, Φ (%) is calculated by following Eq 5 [27]:

$$\boldsymbol{\Phi = \left(1 - \frac{\rho_a}{\rho_b}\right) \times 100\%} \tag{5}$$

in which ρ_a is the apparent density of the RP aerogels (g/cm^3) and ρ_b is the average density of PPF-C and PVA (g/cm^3). The solid density of PVA (1.3 g/cm^3) from Merck and the density of rambutan cellulose (1.224 g/cm^3) were utilized for calculation.

The RP aerogels synthesized under optimal conditions were assessed for their surface area, pore volume, and average pore diameter utilizing the Micromeritics® TriStar II Plus Version 3.03.

The water contact angle of the RP aerogel samples coated with MTMS was determined using an optical contact angle measurement device and analyzed for the surrounding contact line (OCA 20, model ES, DataPhysics, Filderstadt, Germany). Water droplets with a controlled volume of 8 µl were distributed on the surface of the material. Subsequently, contact angle measurement software was utilized to determine the contact angle based on the shape of the water droplets in the image.

2.7. Evaluation of oil adsorption efficiency

The oil adsorption capacity of the aerogel is determined according to ASTM F726-06. First, the aerogels are weighed and then immersed in 300 mL of diesel oil for 2 hours. After soaking, the samples are lifted out of the oil container using a stainless steel mesh basket, drained in the air for 30 seconds to remove excess surface oil, and reweighed [20]. The maximum oil adsorption capacity of the aerogel is calculated using Eq 6:

$$\boldsymbol{Q_m = \frac{m_0 - m_1}{m_0}} \tag{6}$$

where Q_m (g/g) is the maximum oil adsorption capacity of the aerogel, and m_0 (g) and m_1 (g) are the weights of the aerogel before and after the oil adsorption test, respectively.

3. Results and discussion

3.1. Characteristics of cellulose recovered from rambutan peel

The macroscopic evaluation of rambutan peel after two treatment stages is depicted in Figure 1.

The efficacy of the treatment process is observed through the color change of the rambutan peel, where brown is the characteristic color of untreated rambutan peel (Figure 1a) transitioning to white after neutralization with the acid solution during the alkaline treatment stage (Figure 1b). The white color of the final product is a clear indication that nearly pure cellulose material has been recovered.

Figure 1. Surface morphology of RPF-R (a) and RPF-C (b).

The SEM image at ×500 magnification of untreated rambutan peel (Figure 2a) reveals the presence of minerals and non-cellulosic components scattered on the surface [28]. The surface of RPF-R is predominantly composed of a network of lignocellulose and a fibrous matrix containing lignin, cellulose, volatile organic compounds, and hemicellulose [29]. The SEM image of rambutan peel after treatment (Figure 2b) demonstrates the separation of primary cell walls of fibers due to lignin removal during bleaching and hemicellulose removal during alkali treatment. This outcome aligns with findings from Penjumras P, et al.[18].

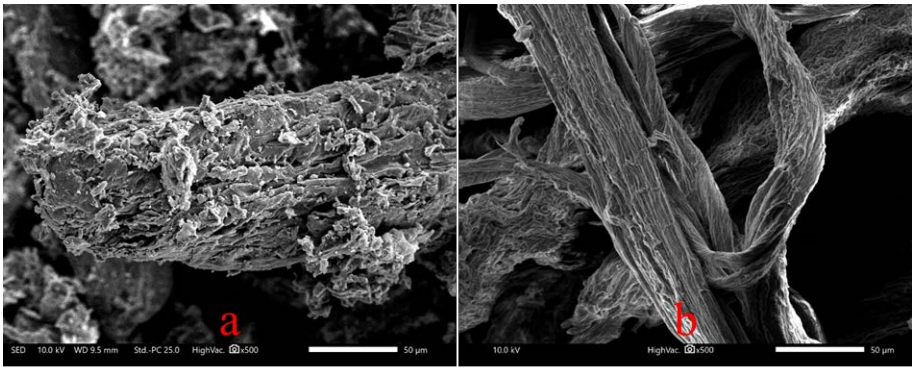

Figure 2. SEM images of RPF-R (a) and RPF-C (b).

3.2. Optimization of the aerogel synthesis process

3.2.1. Experimental design

Table 2 shows the oil adsorption capacity of RP aerogels from 13.4275 g/g to 52.2271 g/g.

Table 2. Experimental design matrix of RP aerogels.

Run	Cellulose content (%wt)	PVA content (%wt)	Ultrasonic time (min)	Ultrasonic power (W)	Oil adsorption capacity (g/g)	
					Experimental	Predicted
1	2	0.1	5	100	19.0193	17.2648
2	1.5	0	10	200	26.2548	28.4046
3	2	0.3	5	100	22.7493	18.2642
4	1.5	0.2	10	200	29.6029	30.104
5	1.5	0.2	10	400	31.3365	30.3566
6	2	0.1	15	300	27.4505	29.0141
7	1.5	0.2	10	200	27.0790	30.104
8	1	0.3	15	300	34.1494	38.1653
9	0.5	0.2	10	200	52.2271	49.6863
10	2	0.1	5	300	28.8128	24.6361
11	1.5	0.2	10	200	32.4801	30.104
12	1.5	0.2	20	200	33.3138	29.5863
13	1.5	0.2	10	200	27.6410	30.104
14	1.5	0.2	0	200	13.4275	19.9227
15	1	0.3	5	300	34.0042	32.0658
16	1	0.1	15	300	42.0983	41.5542
17	1	0.3	15	100	34.9067	34.0542
18	1	0.3	5	100	28.0708	28.7686
19	1.5	0.4	10	200	25.3973	26.0152
20	1.5	0.2	10	0	15.1265	18.8742
21	1.5	0.2	10	200	31.2798	30.104
22	2	0.3	15	300	28.2982	27.9702
23	2	0.3	5	300	23.3516	21.9641
24	2	0.3	15	100	23.1821	23.4563
25	2.5	0.2	10	200	21.3332	26.6417
26	1.5	0.2	10	200	32.5411	30.104
27	2	0.1	15	100	23.9196	20.8288
28	1	0.1	5	300	35.0954	37.0827
29	1	0.1	15	100	30.1228	33.7717
30	1	0.1	5	100	34.8153	30.1142

3.2.2. Analysis of variance (ANOVA)

The results from the analysis of variance (ANOVA) for the quadratic model, as shown in Table 3, confirm that the model equations accurately portray the oil adsorption capacity of RP aerogel within the experimental parameters. The F-values for the respective models stand at 5.99, indicating their significance, with ρ-values below 0.05 signifying the significance of model terms. Specifically, A-Cellulose content (ρ-value < 0.0001), C-Ultrasonic time (ρ-value = 0.0116), D-Ultrasonic power (ρ-value = 0.0039), and A^2 (ρ-value = 0.0217) significantly influence the response (ρ-values < 0.05 and

high F-values). Moreover, the lack of fit F-value of 3.98 and ρ -values exceeding 0.05 suggest that the lack of fit is not significant relative to the pure error.

Table 3. ANOVA of the regression model for the adsorption capacity of RP aerogels.

Source	Sum of Squares	df	Mean Square	F-value	ρ-value	
Model	1423.2	14	101.7	5.99	0.0007	Significant
A-Cellulose content	796.58	1	796.6	46.92	< 0.0001	Significant
B-PVA content	8.56	1	8.56	0.5044	0.4885	
C-Ultrasonic time	140.07	1	140.1	8.25	0.0116	Significant
D-Ultrasonic power	197.77	1	197.8	11.65	0.0039	Significant
AB	5.5	1	5.5	0.3239	0.5777	
AC	0.0087	1	0.009	0.0005	0.9822	
AD	0.1622	1	0.162	0.0096	0.9234	
BC	2.65	1	2.65	0.1561	0.6983	
BD	13.48	1	13.48	0.7939	0.387	
CD	0.6625	1	0.663	0.039	0.8461	
A^2	111.37	1	111.4	6.56	0.0217	
B^2	14.36	1	14.36	0.8457	0.3723	
C^2	49.06	1	49.06	2.89	0.1098	
D^2	51.64	1	51.64	3.04	0.1016	
Residual	254.67	15	16.98			
Lack of Fit	226.23	10	22.62	3.98	0.0704	Not significant
Pure Error	28.44	5	5.69			
Cor Total	1677.8	29				

For the coded equation for oil adsorption capacity depicted in Eq 7, the correlation coefficients R^2 and adjusted R^2 demonstrate a strong correlation, achieving 84.82% and 70.66%.

$$\text{Oil adsorption capacity (g/g)}=30.10–5.76A–0.5974B+2.42C+2.87D+0.5862AB–0.0234AC+0.1007AD+0.4070BC–0.9178BD+0.2035CD+2.02A^2–0.7235B^2–1.34C^2–1.37D^2 \quad (7)$$

Equation 7 can be utilized to predict the oil adsorption capacity of RP aerogel for specific levels of each factor (cellulose content, PVA content, ultrasonic time, and ultrasonic power). By default, the high level of each factor is coded as +1, and the low level is coded as -1. It means that when the oil adsorption capacity increases by +1 unit or decreases by -1 unit, the factors will increase or decrease in accordance with the standardized coefficients associated with that factor.

3.2.3. Optimization of the adsorption process

Table 4 presents the optimal values of factors that yield the optimal oil adsorption capacity values of RP aerogel within the designated scope. Following an assessment of 100 solutions, the optimum conditions were identified as follows: cellulose concentration: 0.540% wt, PVA concentration: 0.122%

wt, ultrasonic time: 12.912 min, and ultrasonic power: 287.837 W. These conditions result in an optimal oil adsorption capacity of 52.301 g/g.

Table 4. The optimal factor values and the corresponding oil adsorption capacity of RP aerogel.

	Unit	Low	High	Optimum
Factors				
Cellulose content	%	0.5	2.5	0.540
PVA content	%	0	0.4	0.122
Ultrasonic time	min	0	20	12.912
Ultrasonic power	W	0	400	287.837
Responses				
Adsorption capacity	g/g			52.301

3.3. Characteristics of aerogel

3.3.1. Morphologies of the sponge aerogel

As depicted in Figure 3, the RPF-R (Figure 1a) were successfully transformed into lightweight porous PF aerogels through an environmentally friendly process using a PVA cross-linker, DI water as the solvent, and a freeze-drying method. The resulting aerogels, based on cellulose extracted from rambutan peel, exhibit a white, porous, and highly lightweight structure.

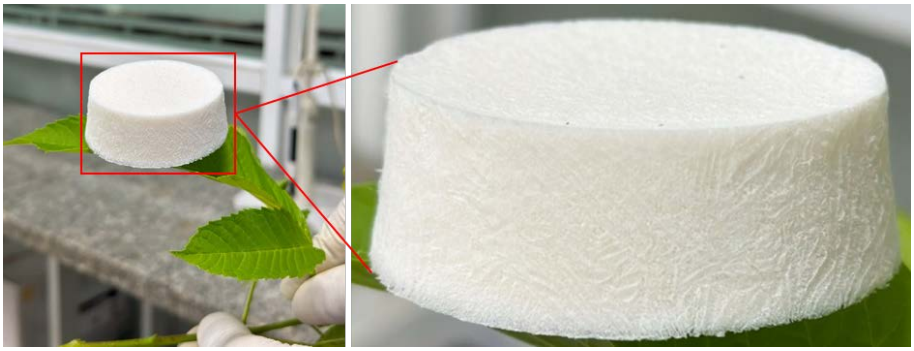

Figure 3. Surface morphology of RP aerogels.

The morphology of RP aerogels was investigated through SEM images shown in Figure 4, indicating that RP aerogels possess an open porous network structure (meaning that there are many extended open space voids) and no clear organization can be observed in the microstructure of the RP aerogels. This suggests that the RPF-C has self-organized and arranged naturally through hydrogen bonds to form three-dimensional porous networks [30].

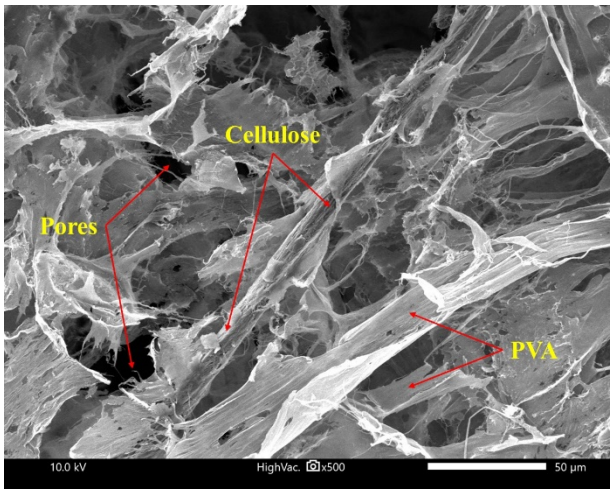

Figure 4. SEM images of the RP aerogels.

Table 5 shows the density of the RP aerogels is 0.027±0.002 g/cm^3, falling within the range observed in various aerogels. For instance, it is lower than densities of straw-derived aerogels (0.05–0.06 g/cm^3) [31], sugarcane bagasse-derived aerogels (0.0473 g/cm^3) [32], and cellulose-based aerogels (0.040 g/cm^3) [33], but higher than those made from wool waste fibers (0.004–0.023 g/cm^3) [34]. RP aerogels also exhibit a high porosity of 97.88±0.19%, consistent with other aerogels such as those from wool waste fibers (97.73–99.63%) [34], pineapple fiber aerogels (96.98–98.85%) [20], corn cob core aerogels (98.13%) [5], and aerogels made from waste paper and banana peels (97.87–98.37%) [6].

Table 5. Density, porosity, and surface areas of the RP aerogel.

Density (g/cm^3)	Porosity (%)	BET surface area (m^2/g)	BJH Adsorption cumulative volume of pores (cm^3/g)	BJH Adsorption average pore width (nm)
0.027±0.002	98.15±0.17	7.5560±0.0735	0.002501	2.0782

Additionally, the BET surface area of RP aerogels is 7.5560±0.0735 m^2/g, with BJH adsorption cumulative volume of pores at 0.002501 cm^3/g, and BJH adsorption average pore width (4V/A) of 20.782 Å (2.0782 nm).

3.3.2. Chemical component of aerogels

To evaluate the surface alteration of RP aerogels, FTIR analysis was performed on uncoated RP aerogels and RP aerogels coated with MTMS (Figure 5).

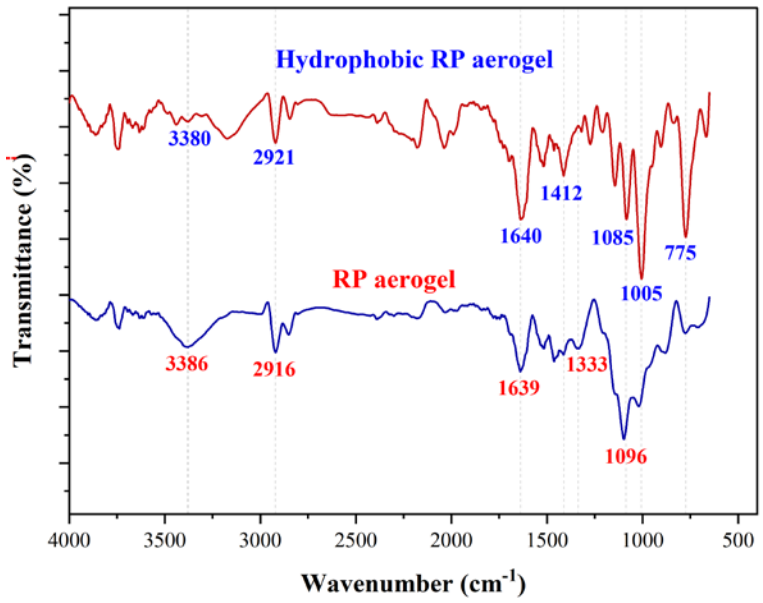

Figure 5. FT-IR of RP aerogels and hydrophobic RP aerogels.

Both RP aerogels and hydrophobic RP aerogels exhibit characteristic bands in the cellulose molecule (Figure 5). Specifically, the broad intensity bands at 3386 cm^{-1} and 3380 cm^{-1} represent the hydrogen bonding (–OH) of PVA [18], indicating the presence of PVA in RP aerogels and hydrophobic RP aerogels as a cross-linking agent. The observed vibrational bands around 2921 cm^{-1} and 2916 cm^{-1} are attributed to the symmetric and asymmetric stretching vibrations of the –CH bonds in the alkyl groups (CH_2) found in the PVA and cellulose chains [34]. The broad intensity bands at 1640 cm^{-1} and 1639 cm^{-1} are characteristic of the C=C (benzene ring) group [35]. The broad intensity bands at 1412 cm^{-1} and 1333 cm^{-1} correspond to the O–H bending (alcohol) group [36], while the bands at 1096 cm^{-1} and 1085 cm^{-1} are indicative of the stretching vibrations of C–O–C [27]. Additionally, it is noteworthy that hydrophobic RP aerogels exhibit a new peak at 1005 cm^{-1}, characteristic of the stretching vibrations of Si–O–Si bonds [27], and a peak at 775 cm^{-1} representing the vibration of Si-C bonds [37]. It can be concluded that a strong cross-linked Si-O-Si layer is formed via the hydrolysis-condensation process of MTMS [38]. After salinization, the -OH groups are replaced by –O–Si–$(CH_3)_3$ groups from MTMS, resulting in the hydrophobic properties of the RP aerogels coated with MTMS [20].

3.3.3. Wettability

MTMS-coated RP aerogels exhibit excellent hydrophobic properties, with a water contact angle measured up to 152.7° (Figure 6).

Figure 6. The water contact angle on the surface of RP aerogels coated with MTMS.

After being coated with MTMS, a strong, cross-linked layer of Si-O-Si bonds is formed through chemical bonding by MTMS via the chemical vapor deposition process [38]. The water contact angle of RP aerogels is higher compared to other hydrophobic aerogel materials such as pineapple fiber aerogels (146.1°) [20] and aerogels from wool waste fibers (138°) [34], but lower than cellulose-based aerogels from water hyacinth stems (*Eichhornia crassipes*) (154.8°) [39] and straw aerogels (151±7°) [40].

4. Conclusion

In this research, eco-friendly aerogels have been successfully fabricated from recycled cellulose fibers derived from rambutan peel waste. The resultant RP aerogels exhibit characteristic white coloration post-bleaching, extremely low density (0.027±0.002 g/cm^3), high porosity (97.88±0.19%), and remarkable hydrophobicity (water contact angle of 152.7°). The surface area of the synthesized aerogels was also determined, with a BET surface area of 7.5560±0.0735 m^2/g, BJH adsorption cumulative pore volume of 0.002501 cm^3/g, and BJH adsorption average pore width of 2.0782 nm. Through surface response analysis utilizing experimental design modeling with 30 trials, optimal synthesis conditions for aerogels were established: cellulose content: 0.540%wt, PVA content: 0.122%wt, ultrasonic power: 12.912 min, and ultrasonic time: 287.837W. Under these specified conditions, the optimal oil adsorption capacity is 52.301g/g. Rambutan peel holds great promise as one of the potential materials for creating effective, environmentally friendly, and efficient adsorbents in the future.

Use of AI tools declaration

The authors declare they have not used Artificial Intelligence (AI) tools in the creation of this article.

Acknowledgments

This research was fully funded by HUTECH University under grant number 239/HĐ-ĐKC and the AKIHIKO IKAI Family Scholarship Fund.

Conflict of interest

All authors declare no conflicts of interest in this paper.

References

1. Kolokoussis P, Karathanassi V (2018) Oil spill detection and mapping using sentinel 2 imagery. *J Mar Sci Eng* 6: 1–12. https://doi.org/10.3390/jmse6010004
2. Alaa El-Din G, Amer AA, Malsh G, et al. (2018) Study on the use of banana peels for oil spill removal. *Alex Eng J* 57: 2061–2068. https://doi.org/10.1016/j.aej.2017.05.020
3. Banerjee SS, Joshi MV, Jayaram RV (2006) Treatment of oil spill by sorption technique using fatty acid grafted sawdust. *Chemosphere* 64: 1026–1031. https://doi.org/10.1016/j.chemosphere.2006.01.065
4. Loh J, Goh X, Nguyen P, et al. (2022) Advanced Aerogels from Wool Waste Fibers for Oil Spill Cleaning Applications. *J Environ Polym Degrad* 30: 1–14. https://doi.org/10.1007/s10924-021-02234-y
5. Peng D, Zhao J, Liang X, et al. (2023) Corn stalk pith-based hydrophobic aerogel for efficient oil sorption. *J Hazard Mater* 448: 130954. https://doi.org/10.1016/j.jhazmat.2023.130954
6. Chung VN, Nguyen TS, Huynh KPH, et al. (2022) Fabrication of Cellulose Aerogel from Waste Paper and Banana Peel for Water Treatment. *Chem Eng Trans* 97: 337–342. https://doi.org/10.3303/CET2297057
7. Luu TP, Do NHN, Chau NDQ, et al. (2020) Morphology Control and Advanced Properties of Bio-Aerogels from Pineapple Leaf Waste. *Chem Eng Trans* 78: 433–438. https://doi.org/10.3303/CET2078073
8. Yen TD, Nga HND, Phuong TXN, et al. (2022) Green fabrication of bio-based aerogels from coconut fibers for wastewater treatment. *J Porous Mater* 29: 1–14. https://doi.org/10.1007/s10934-022-01257-7
9. Tripathi P, Karunakaran G, Sakthivel T, et al. (2021) Status and prospects of rambutan cultivation in India. *Acta Horticulturae* 1293: 33–40. https://doi.org/10.17660/ActaHortic.2020.1293.5
10. Department of Horticulture: Handbook of farming techniques according to VietGAP for 10 major fruit trees. Ministry of Agriculture and Rural Development of Vietnam, 2022. Available from: https://s.net.vn/oPpa
11. Buu BC: Vietnam agriculture in 2023 shifting to intelligent production. Institute of Agricultural Science for Southern Vietnam, 2024. Available from: https://s.net.vn/sUL2

12. Oliveira E, Santos J, Goncalves AP, et al. (2016) Characterization of the Rambutan Peel Fiber (*Nephelium lappaceum*) as a Lignocellulosic Material for Technological Applications. *Chem Eng Trans* 50: 391–396. https://doi.org/10.3303/CET1650066
13. Draper NR, John JA (1988) Response-Surface Designs for Quantitative and Qualitative Variables. *Technometrics* 30: 423–428. https://doi: 10.1080/00401706.1988.10488437
14. Li X, Zhu W, Wang B, et al. (2023) Optimization of cooling water jacket structure of high-speed electric spindle based on response surface method. *Case Stud Therm Eng* 48: 103158. https://doi.org/10.1016/j.csite.2023.103158
15. Bradley N (2007) The response surface methodology. Master's Thesis Indiana University of South Bend.
16. Bayuo J, Pelig-Ba KB, Abukari MA (2019) Optimization of Adsorption Parameters for Effective Removal of Lead (II) from Aqueous Solution. *Physical Chemistry: An Indian Journal* 14: 1–25.
17. Meng Y, Wang X, Wu Z, et al. (2015) Optimization of cellulose nanofibrils carbon aerogel fabrication using response surface methodology. *Eur Polym J* 73: 137–148. https://doi.org/10.1016/j.eurpolymj.2015.10.007
18. Penjumras P, Abdul Rahman R, Talib RA, et al. (2014) Extraction and Characterization of Cellulose from Durian Rind. *Agric Agric Sci Procedia* 2: 237–243. https://doi.org/10.1016/j.aaspro.2014.11.034
19. Nguyen TTV, Tri N, Tran BA, et al. (2021) Synthesis, Characteristics, Oil Adsorption, and Thermal Insulation Performance of Cellulosic Aerogel Derived from Water Hyacinth. *ACS Omega* 6: 26130–26139. https://doi.org/10.1021/acsomega.1c03137
20. Nga HND, Thao PL, Quoc BT, et al. (2019) Advanced fabrication and application of pineapple aerogels from agricultural waste. *Mater Technol* 35: 1–8. https://doi.org/10.1080/10667857.2019.1688537
21. Thai QB, Nguyen ST, Ho DK, et al. (2019) Cellulose-based aerogels from sugarcane bagasse for oil spill-cleaning and heat insulation applications. *Carbohydr Polym* 228: 115365. https://doi.org/10.1016/j.carbpol.2019.115365
22. Salehi M, Sefti M, Moghadam A, Koohi A (2012) Study of Salinity and pH Effects on Gelation Time of a Polymer Gel Using Central Composite Design Method. *J Macromol Sci B* 51: 438–451. https://doi.org/10.1080/00222348.2011.597331.
23. Mourabet M, El Rhilassi A, El Boujaady H, et al. (2017) Use of response surface methodology for optimization of fluoride adsorption in an aqueous solution by Brushite. *Arab J Chem* 10: S3292–S3302. https://doi.org/10.1016/j.arabjc.2013.12.028
24. Owolabi RU, Usman MA, Kehinde AJ (2018) Modelling and optimization of process variables for the solution polymerization of styrene using response surface methodology. *J King Saud Univ Eng Sci* 30: 22–30. https://doi.org/10.1016/j.jksues.2015.12.005
25. Markowska-Szczupak A, Wesołowska A, Borowski T, et al. (2022) Effect of pine essential oil and rotating magnetic field on antimicrobial performance. *Sci Rep* 12: 9712. https://doi.org/10.1038/s41598-022-13908-5.

26. Tazik M, Dehghani MH, Yaghmaeian K, et al. (2023) 4-Chlorophenol adsorption from water solutions by activated carbon functionalized with amine groups: response surface method and artificial neural networks. *Sci Rep* 13: 7831. https://doi.org/10.1038/s41598-023-35117-4.
27. Shi G, Qian Y, Tan F, et al. (2019) Controllable synthesis of pomelo peel-based aerogel and its application in adsorption of oil/organic pollutants. *R Soc Open Sci* 6: 181823. https://doi.org/10.1098/rsos.181823
28. Mandal A, Chakrabarty D (2011) Isolation of nanocellulose from waste sugarcane bagasse (SCB) and its characterization. *Carbohydr Polym* 86: 1291–1299. https://doi.org/10.1016/j.carbpol.2011.06.030
29. Nguyen TT, Loc ND, Ba LH, et al. (2023) Efficient oil removal from water using carbonized rambutan peel: Isotherm and kinetic studies. *Vietnam J Hydrometeorol* 4: 1–18. https://doi.org/10.36335/VNJHM.2023(17).1-18
30. Nguyen S, Feng J, Ng S, et al. (2014) Advanced thermal insulation and absorption properties of recycled cellulose aerogels. *Colloids Surf A: Physicochem Eng Asp* 445: 128–134. https://doi.org/10.1016/j.colsurfa.2014.01.015
31. Du TT, Son TN, Nam Duc Do, et al. (2020) Green aerogels from rice straw for thermal, acoustic insulation and oil spill cleaning applications. *Mater Chem Phys* 253: 123363. https://doi.org/10.1016/j.matchemphys.2020.123363
32. Li W, Li Z, Wang W, et al. (2021) Green approach to facilely design hydrophobic aerogel directly from bagasse. *Ind Crops Prod* 172: 113957. https://doi.org/10.1016/j.indcrop.2021.113957
33. Nguyen ST, Feng J, Le NT (2013) Cellulose Aerogel from Paper Waste for Crude Oil Spill Cleaning. *Ind Eng Chem Res* 52: 18386–18391. https://doi.org/10.1021/ie4032567
34. Loh J, Goh X, Nguyen P, et al. (2022) Advanced Aerogels from Wool Waste Fibers for Oil Spill Cleaning Applications. *J Environ Polym Degrad* 30: 1–14. https://doi.org/10.1007/s10924-021-02234-y
35. Lv P, Almeida G, Perré P (2015) TGA-FTIR Analysis of Torrefaction of Lignocellulosic Components (cellulose, xylan, lignin) in Isothermal Conditions over a Wide Range of Time Durations. *BioResources* 10: 4239–4251. https://doi.org/10.15376/biores.10.3.4239-4251
36. Kumar N, Pruthi V (2015) Structural elucidation and molecular docking of ferulic acid from Parthenium hysterophorus possessing COX-2 inhibition activity. *3 Biotech* 5: 541–551. https://doi.org/10.1007/s13205-014-0253-6
37. Chau NDQ, Nghiem TTN, Doan HLX, et al. (2020) Advanced Fabrication and Applications of Cellulose Acetate Aerogels from Cigarette Butts. *Mater Trans* 61: 1550–1554. https://doi.org/10.2320/matertrans.MT-MN2019009
38. Xiao S, Gao R, Lu Y, et al. (2015) Fabrication and characterization of nanofibrillated cellulose and its aerogels from natural pine needles. *Carbohydr Polym* 119. https://doi.org/10.1016/j.carbpol.2014.11.041
39. Yin T, Zhang X, Liu X, et al. (2016) Cellulose-based aerogel from Eichhornia crassipes as an oil superabsorbent. *RSC Adv* 6: 98563–98570. https://doi.org/10.1039/C6RA22950F

40. Dilamian M, Noroozi B (2021) Rice straw agri-waste for water pollutant adsorption: Relevant mesoporous super hydrophobic cellulose aerogel. *Carbohydr Polym* 251: 117016. https://doi.org/10.1016/j.carbpol.2020.117016